

# Nanoscale

Accepted Manuscript



This is an *Accepted Manuscript*, which has been through the Royal Society of Chemistry peer review process and has been accepted for publication.

*Accepted Manuscripts* are published online shortly after acceptance, before technical editing, formatting and proof reading. Using this free service, authors can make their results available to the community, in citable form, before we publish the edited article. We will replace this *Accepted Manuscript* with the edited and formatted *Advance Article* as soon as it is available.

You can find more information about *Accepted Manuscripts* in the [Information for Authors](#).

Please note that technical editing may introduce minor changes to the text and/or graphics, which may alter content. The journal's standard [Terms & Conditions](#) and the [Ethical guidelines](#) still apply. In no event shall the Royal Society of Chemistry be held responsible for any errors or omissions in this *Accepted Manuscript* or any consequences arising from the use of any information it contains.

## ARTICLE

# Engineering Defect State and Reducibility of Ceria Based Nanoparticles for Improved Anti-oxidation Performance

Cite this: DOI:  
10.1039/x0xx00000x

Received 00th January 2012,  
Accepted 00th January 2012

DOI: 10.1039/x0xx00000x

[www.rsc.org/](http://www.rsc.org/)

Yan-Jie Wang,<sup>a,b</sup> Hao Dong,<sup>a</sup> Guang-Ming Lyu,<sup>a</sup> Huai-Yuan Zhang,<sup>a</sup> Jun Ke,<sup>a</sup> Li-Qun Kang,<sup>a</sup> Jia-Li Teng,<sup>c</sup> Ling-Dong Sun,<sup>a,\*</sup> Rui Si,<sup>d</sup> Jing Zhang,<sup>e</sup> Yan-Jun Liu,<sup>c,\*</sup> Ya-Wen Zhang,<sup>a</sup> Yun-Hui Huang<sup>b,\*</sup> and Chun-Hua Yan<sup>a,\*</sup>

Due to the excellent anti-oxidation performance, CeO<sub>2</sub> nanoparticles receive wide attention in pharmacological application. Deep understanding of anti-oxidation mechanism is extremely important to develop potent CeO<sub>2</sub> nanomaterials for anti-oxidation application. Here, we report the detailed study on the anti-oxidation process of CeO<sub>2</sub> nanoparticles. The valence state and coordination structure of Ce are characterized before and after the addition of H<sub>2</sub>O<sub>2</sub> to understand the anti-oxidation mechanism of CeO<sub>2</sub> nanoparticles. Adsorbed peroxide species are detected during the anti-oxidation process, which is responsible for the red-shifted UV-vis absorption spectra of CeO<sub>2</sub> nanoparticles. Furthermore, the coordination number of Ce in the first coordination shell slightly increased after the addition of H<sub>2</sub>O<sub>2</sub>. On the basis of these experimental results, the reactivity of coordination sites for peroxides species is considered to play as a key role in the anti-oxidation performance of CeO<sub>2</sub> nanoparticles. Furthermore, we present a robust method to engineer the anti-oxidation performance of CeO<sub>2</sub> nanoparticles through the modification of defect state and reducibility by doping with Gd<sup>3+</sup>. The improved anti-oxidation performance is also observed in cell culture, where the biocompatible CeO<sub>2</sub>-based nanoparticles can protect INS-1 cells from oxidative stress induced by H<sub>2</sub>O<sub>2</sub>, suggesting the potential application of CeO<sub>2</sub> nanoparticles in the treatment of diabetes.

## Introduction

Many diseases, like ageing, ischemia/reperfusion injury, atherosclerosis, neurodegenerative diseases (Alzheimer's disease and Parkinson's disease), and diabetes, are closely related to reactive oxygen species (ROS) produced by the aerobic metabolism.<sup>1-5</sup> Excess ROS would damage deoxyribonucleic acid (DNA), proteins, and lipids, and thus lead to cell malfunction, apoptosis, and tissue damage.<sup>6</sup> Therefore, the anti-oxidant capacity of human tissue is vital for human health. During the past few decades, antioxidant therapies, such as vitamin E and vitamin C's application in the treatment of oxidative stress models.<sup>7-9</sup> However, these small molecules are inherently unstable, and possess limited active sites. Development of effective antioxidants is active area in the therapeutic research of ROS related diseases. Recently, redox-

active metal oxide nanoparticles (NPs) are found to be more favorable, by virtue of their rich active sites and excellent stability.<sup>10</sup> Among them, ceria NPs have attracted great interest for their outstanding redox properties.

In ceria, the formation and depletion of oxygen vacancies can occur with the conversion between Ce<sup>4+</sup> and Ce<sup>3+</sup> depending on the oxygen partial pressure in the surrounding atmosphere.<sup>11,12</sup> This ability is critical in the diverse applications of ceria including oxygen sensors, CO catalytic oxidation and water-gas shift catalysis.<sup>13-18</sup> Ceria NPs show outstanding chemical activity due to more oxygen vacancies on the particle surface and high specific surface area compared to bulk ceria.<sup>19-23</sup> Biologically, since oxygen vacancies on the surface can act as active sites for free radical scavenging, ceria NPs exhibit

excellent anti-oxidation performance in protecting cells from radiation, inflammation, ischemic strokes and so on.<sup>24-27</sup> However, there are many uncertain factors in complex biological systems. Therefore, the anti-oxidation mechanism of ceria NPs, which is the basis of biological application, remains unclear. Importantly, a deep understanding of the anti-oxidation mechanism is significant to the design and modulation of active sites for developing advanced antioxidants and anti-oxidation applications.

Many researches have been conducted on the anti-oxidation performance of ceria NPs. Self and coworkers reported ceria NPs exhibit superoxide dismutase (SOD) activity and catalase mimetic activity.<sup>28-30</sup> Zhou *et al.* investigated the hydroxyl radical scavenging activity of CeO<sub>2</sub> NPs using methyl violet.<sup>31</sup> In addition, the modulation of anti-oxidation performance by tuning the size and shape of the ceria NPs and the conversion between Ce<sup>3+</sup> and Ce<sup>4+</sup> has been reported.<sup>32-37</sup> Colvin *et al.* studied on the effect of size and surface coating on the anti-oxidant capacity of ceria NPs.<sup>32</sup> Ma *et al.* constructed a novel nano-complex (apoferritin–CeO<sub>2</sub>) with most active artificial redox enzyme with mimetic SOD activity.<sup>34</sup> Seal *et al.* tuned the regeneration of active centers of CeO<sub>2</sub> NPs by polyethylene glycol coating.<sup>37</sup> Furthermore, there are some contradictory results in the previous works about the active sites of ceria NPs and the anti-oxidation process.<sup>28-33</sup> However, few studies focused on monitoring the anti-oxidation process, which is important for a deep understanding of the anti-oxidation mechanism and delicate designs of the active sites of CeO<sub>2</sub> NPs. There are many unresolved questions about the anti-oxidation mechanism of ceria NPs, such as how absorption spectrum, medium species, coordination environment and surface state evolve during the anti-oxidation process.<sup>32</sup> Therefore, probing the anti-oxidation process of CeO<sub>2</sub> NPs is significant in understanding the anti-oxidation mechanism in order to reveal their active centers. Moreover, the modulation of active centers in CeO<sub>2</sub> NPs will draw a broad attention for further bio-applications.<sup>34-38</sup>

Here, we monitored the anti-oxidation process of CeO<sub>2</sub> NPs with H<sub>2</sub>O<sub>2</sub> and engineered the anti-oxidation performance by Gd<sup>3+</sup> doping. The main valence state of surface Ce in the sample as determined by X-ray photoelectron spectroscopy (XPS) is +4. The reaction between CeO<sub>2</sub> NPs and H<sub>2</sub>O<sub>2</sub> was studied with UV-vis absorption spectroscopy, X-ray absorption fine structure (XAFS) and Raman spectroscopy. Adsorbed peroxide species were observed during the anti-oxidation process. The effect of extra OH<sup>-</sup> or H<sup>+</sup> was also investigated to deeply understand the anti-oxidation mechanism of CeO<sub>2</sub> NPs. In addition, a red-shift in the absorption spectrum of CeO<sub>2</sub> NPs was observed after adding H<sub>2</sub>O<sub>2</sub>, and the extent of the red-shift was related to the percentage of Gd<sup>3+</sup> dopant. Moreover, in the probe reaction with H<sub>2</sub>O<sub>2</sub>, the anti-oxidation capability of CeO<sub>2</sub> NPs was improved by Gd<sup>3+</sup> doping. The anti-oxidation performance of CeO<sub>2</sub> and Gd<sup>3+</sup> doped CeO<sub>2</sub> (CeO<sub>2</sub>:Gd) NPs in protecting INS-1 cells against oxidative stress induced by H<sub>2</sub>O<sub>2</sub> was also assessed in cell culture.

## Experimental

### Chemicals and reagents

Ce(NO<sub>3</sub>)<sub>3</sub>·6H<sub>2</sub>O (99%, Sinopharm Chemical Corp., China), Gd<sub>2</sub>O<sub>3</sub> (> 99.5%, Minmetals Rare Earth Corp., China), NaOH (A.R. Beijing Chemical Corp., China), HNO<sub>3</sub> (A.R. Beijing Chemical Corp., China), H<sub>2</sub>O<sub>2</sub> (A.R. Beijing Chemical Corp., China), H<sub>2</sub>SO<sub>4</sub> (A.R. Beijing Chemical Corp., China), and KMnO<sub>4</sub> (A.R. Beijing Chemical Corp., China) were used as received.

### Synthesis of CeO<sub>2</sub> and CeO<sub>2</sub>:Gd NPs

All CeO<sub>2</sub>-based materials were prepared by a modified hydrothermal method.<sup>39</sup> Gd(NO<sub>3</sub>)<sub>3</sub> was prepared from reaction between Gd<sub>2</sub>O<sub>3</sub> and HNO<sub>3</sub>. To obtain CeO<sub>2</sub> NPs, 0.75 mmol Ce(NO<sub>3</sub>)<sub>3</sub>·6H<sub>2</sub>O and 1.5 mmol NaOH were dissolved in distilled water. Gd(NO<sub>3</sub>)<sub>3</sub> solution was introduced to prepared CeO<sub>2</sub>:Gd NPs. The total volume of the suspension was adjusted to 15 mL. After being stirred at room temperature for 30 min, the mixed suspension was transferred into a Teflon-lined stainless steel autoclave and heated at 120 °C for 24 h. The products were collected by centrifugation, washed with deionized water, and redispersed in water for use.

### Instrument and characterization

X-ray diffraction (XRD) patterns of dried powders were measured on a D/MAX-2000 diffractometer (Rigaku, Japan) with a slit of 1/2° at a scanning speed of 4° min<sup>-1</sup> using Cu K $\alpha$  radiation. For transmission electron microscopy (TEM) analysis, the samples were prepared by dispersing the products in water and drying a droplet of the suspension on copper grids coated with holey carbon membranes. The TEM micrograph was taken by a JEOL JEM2100 transmission electron microscope operating at 200 kV with a single tilt holder (Japan) to observe particle size and shape. Inductively coupled plasma-atomic emission spectroscopy (ICP-AES) analysis was performed with a Profile Spec ICP-AES spectrometer (Leeman, U.S.A.). X-ray photoelectron spectroscopy (XPS) analysis was performed with an Axis Ultra XPS spectrometer (Kratos, U.K.) with 225 W of Al K $\alpha$  radiation. The C 1s line at 284.8 eV was used to calibrate the binding energies (BE). Electron Energy Loss Spectroscopy (EELS) was obtained by Tecnai F30 operating at 200 kV. Thermogravimetric analysis (TGA) was taken on Q600SDT. FT infrared spectroscopy (FT-IR) was operated on VECT22. Temperature programmed reduction with H<sub>2</sub> (H<sub>2</sub>-TPR) analysis was performed by ramping 100 mg of as-prepared samples up to 700°C (10°C/min) in H<sub>2</sub> (5 vol%)/He flow (40 mL/min). H<sub>2</sub> consumption was analyzed by a thermos conductivity detector (TCD). Dynamic light scattering (DLS) measurements were carried out on a nanoparticle analyzer SZ-100 (HORIBA). Raman spectra were collected on a Jobin-Yvon HR800 Laser Raman Microscope under 488 nm laser excitation. Brunauer-Emmett-Teller (BET) specific surface area of the samples calcined at 120 °C in vacuum was measured via nitrogen adsorption at 77 K on an ASAP-2010 analysis system (Micro meritics, U.S.A.). Electron spin-resonance spectroscopy

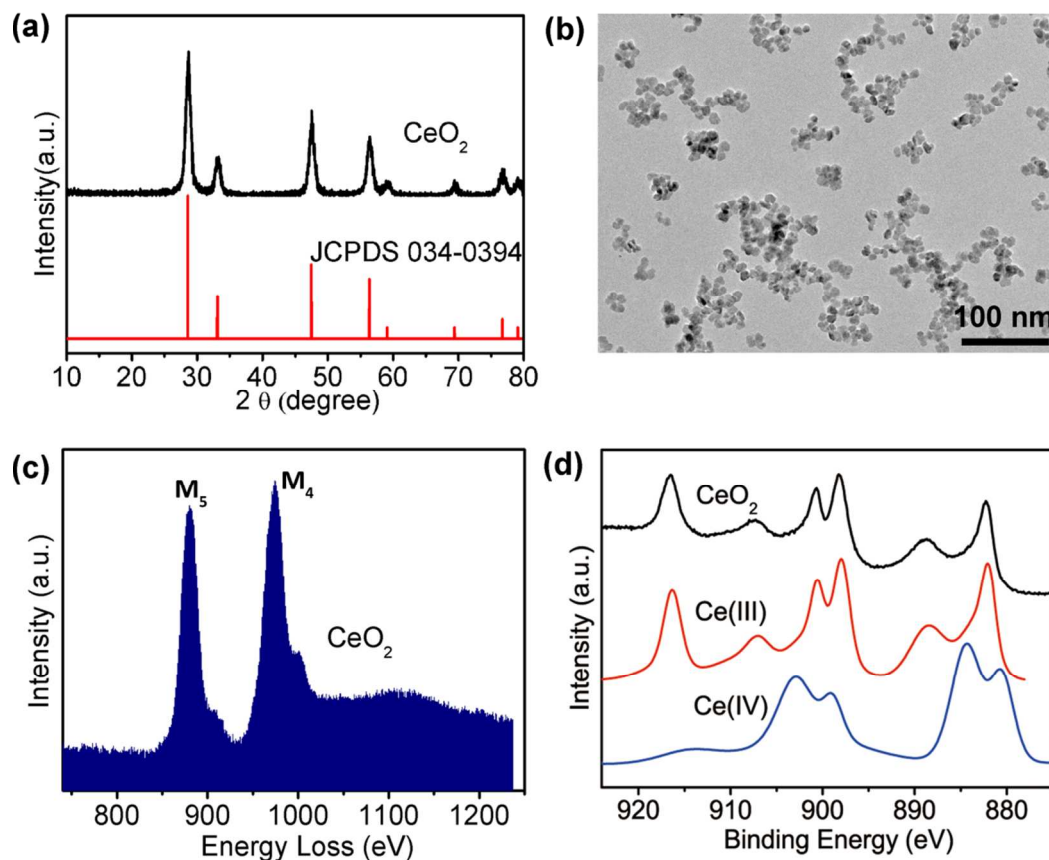


**Fig. 1** Characterization of CeO<sub>2</sub> NPs. (a) XRD pattern of as-prepared CeO<sub>2</sub> NPs. (b) TEM image of as-prepared CeO<sub>2</sub> NPs. (c) EEL spectrum of as-prepared CeO<sub>2</sub> NPs. (d) Ce 3d XPS spectrum of as-prepared CeO<sub>2</sub> NPs. Ce(III): Ce 3d XPS spectrum of Ce<sup>3+</sup>, Ce(IV): Ce 3d XPS spectrum of Ce<sup>4+</sup>.

(ESR) was measured using a Bruker model ER 4122SHQE super high Q resonator. The samples for ESR measurement was prepared at room temperature and loaded into capillary quartz tubes immediately after mixing of reagents.

### UV–vis Spectroscopy

In order to probe the anti-oxidation reaction of CeO<sub>2</sub> NPs with H<sub>2</sub>O<sub>2</sub>, UV–vis absorption spectra were obtained using UV3100 Spectrometer (Shimadzu). 4 mL H<sub>2</sub>O<sub>2</sub> was mixed with 1 mL 500 μg/mL CeO<sub>2</sub> solution (H<sub>2</sub>O<sub>2</sub>/Ce ratio was 0, 0.02, 0.03, 0.04, 0.1, 0.25, 0.5, 1.0, 2.0, 4.0, 8.0, 16.0, 32.0, 57.0, respectively). Then the UV–vis absorption spectra of above mixed solution were measured in time.

### In situ Raman Spectroscopy

Raman spectra were collected on a Jobin-Yvon HR800 Laser Raman Microscope with 488 nm laser excitation. Before the measurement, the sample containing 80 mg CeO<sub>2</sub> and 60 mg H<sub>2</sub>O<sub>2</sub> in 0.4 mL distilled water was smeared on the glass sheet. We tested continuously the Raman shift of the as-prepared sample at the reaction time of 0, 5, 10, 30, 60, and 180 min.

### XAFS measurement

The quick-scanning XAFS (QXAFS) analysis was performed on the 1W2B beam line of the Beijing Synchrotron Radiation Facility (BSRF) operated at 2.2 GeV with injection current of 140–300 mA. The Ce L<sub>3</sub>-edge absorption spectra of the samples were measured in transmission mode. It took about 1 min to obtain one spectrum. For each data, the spectra collection was performed 10 times to increase the independent points, so as to decrease the fitting error in the data analysis. The XAFS spectra of CeO<sub>2</sub> sample were collected during the reaction with H<sub>2</sub>O<sub>2</sub> at the reaction time of 0 min, 10 min, 30 min, 3 h and 9 h. Athena and Artemis codes were used to extract the data and to fit the curves with the reported model, respectively. The Fourier transformed curves were fitted in real space with  $\Delta k = 2.2 - 9.6 \text{ \AA}^{-1}$  and  $\Delta R = 1.4 - 3.1 \text{ \AA}$  for Ce ( $\kappa^2$  weighted).

### Anti-oxidation capacity of CeO<sub>2</sub>-based NPs in the decomposition of H<sub>2</sub>O<sub>2</sub>

80 μL H<sub>2</sub>O<sub>2</sub> (100 μg/mL) was injected to 20 μL CeO<sub>2</sub>-based NPs aqueous solution (500 μg/mL) in 96 well plate, and the mixed solution was handled at 37 °C. To measure the residual concentration of H<sub>2</sub>O<sub>2</sub> in the solution, 50 μL H<sub>2</sub>SO<sub>4</sub> (9.0 mol/L) and 50 μL KMnO<sub>4</sub> (3.2 mmol/L) were added to the reaction solution sequentially. Finally the absorbance at 525 nm was tested on a

microplate spectrophotometer. This experiment was repeated in triplicate.

### Cell Culture

INS-1 cells were purchased from China Center for typical culture collection. INS-1 cells were grown at 37 °C in RPMI 1640 medium (Gibco Corp., America) supplemented with 10% fetal bovine serum (FBS) (Gibco Corp., America), 2mol/L L-glutamine, 100 IU/mL penicillin and streptomycin, in a humidified atmosphere of 5% CO<sub>2</sub> in air. All experiments were performed on cells in the logarithmic phase of growth under condition of  $\geq 98\%$  viability. Cell viability was evaluated by CCK-8 assay (Dojindo Corp., Japan). INS-1 cells were seeded in 96-well tissue culture plates at the density of 8000 cells per well and incubated two days. Then 100  $\mu\text{g/mL}$  CeO<sub>2</sub>-based NPs were added. After 2 h, 100  $\mu\text{mol/L}$  H<sub>2</sub>O<sub>2</sub> was injected. Then, the original medium was removed and 120  $\mu\text{L}$  fresh medium containing 10  $\mu\text{L}$  CCK8 was added after 30 min. Incubating for another 2 h at 37 °C, the absorbance of each well was collected to calculate the cell viability.

### Results and discussion

A deep understanding of the anti-oxidation mechanism is significant to the design and modulation of active sites for developing potent antioxidants and anti-oxidation applications. The underlying anti-oxidation mechanism of ceria nanomaterials has been unclear.<sup>24,30-34</sup> Therefore, it is important to study the anti-oxidation of ceria nanomaterials.

In this work, CeO<sub>2</sub> NPs used in the investigation of anti-oxidation mechanism were prepared by a simple hydrothermal method.<sup>39</sup> Requisite characterizations were carried out in order to understand the structure and surface properties of as-prepared CeO<sub>2</sub> NPs. As shown in XRD patterns (Fig. 1a), the diffraction peaks of as-prepared CeO<sub>2</sub> NPs are well indexed to the pure fluorite cubic structures (JCPDS 034-0394), and no other phase or component is observed. From the TEM image shown in Fig. 1b, the morphology of CeO<sub>2</sub> NPs is torispherical, and the size of as-prepared CeO<sub>2</sub> NPs ranges from 4 to 10 nm (Fig. S1 in ESI†), consistent with the calculated result using Scherrer equation (Table S1 in ESI†). Moreover, the corresponding interplanar spacing (*d*) obtained from HRTEM images (Fig. S2 in ESI†) agrees well with the standard *d* value of 0.312 nm for cubic CeO<sub>2</sub>. To understand the chemical state of CeO<sub>2</sub> NPs, EELS was carried out. EELS of as-prepared CeO<sub>2</sub> NPs shown in Fig. 1c is close to that of bulk CeO<sub>2</sub> (Fig. S3 in ESI†). And the detailed analysis of Ce<sup>3+</sup> percentage through M<sub>5</sub>/M<sub>4</sub> intensity ratio is shown in Fig. S3. In order to find out the valence state of surface Ce in as-prepared CeO<sub>2</sub> NPs, XPS analysis was conducted. Ce 3d XPS spectrum (Fig. 1d) is close to that of Ce<sup>4+</sup>, indicating that the main valence of surface Ce in the sample is +4. The detailed analysis of Ce 3d XPS is shown in Fig. S4 in ESI†.<sup>40-44</sup> In addition, FT infrared spectroscopy (FT-IR) and thermo gravimetric analysis (TGA) of CeO<sub>2</sub> NPs shown in Fig. S5 in ESI† indicate the presence of

surface bonded-OH radicals on the CeO<sub>2</sub> NPs surface due to the basic environment from the synthesis procedure.<sup>45</sup>

### Anti-oxidation process of CeO<sub>2</sub> NPs

The underlying anti-oxidation mechanism of ceria nanomaterials remains unclear in such aspects as indefinite active center, unclear reaction process and so on.<sup>24,30-34</sup> The investigation on the interaction between ceria and ROS is significant to reveal the anti-oxidation mechanism and develop potent anti-oxidants. In this regard, it is necessary to probe the coordination environment, medium species and surface state during the anti-oxidation process of CeO<sub>2</sub> NPs. Here, H<sub>2</sub>O<sub>2</sub> was chosen as a typical ROS in the research on the anti-oxidation mechanism of CeO<sub>2</sub> NPs. We examined the coordination structures, adsorbed oxygen species and valence state during the anti-oxidation process of CeO<sub>2</sub> NPs.

The color of CeO<sub>2</sub> NPs solution changed to yellow from colorless with H<sub>2</sub>O<sub>2</sub> addition. Meanwhile, the red-shifted absorption spectra of CeO<sub>2</sub> NPs are observed with the addition of H<sub>2</sub>O<sub>2</sub> (Fig 2a) similar to the previous report<sup>32</sup>. Moreover, as illustrated in Fig. 2b, the red shift increases with the H<sub>2</sub>O<sub>2</sub>/Ce ratio from 0 to 57. As known, the shift of absorption is dependent on the physical and chemical properties of ceria

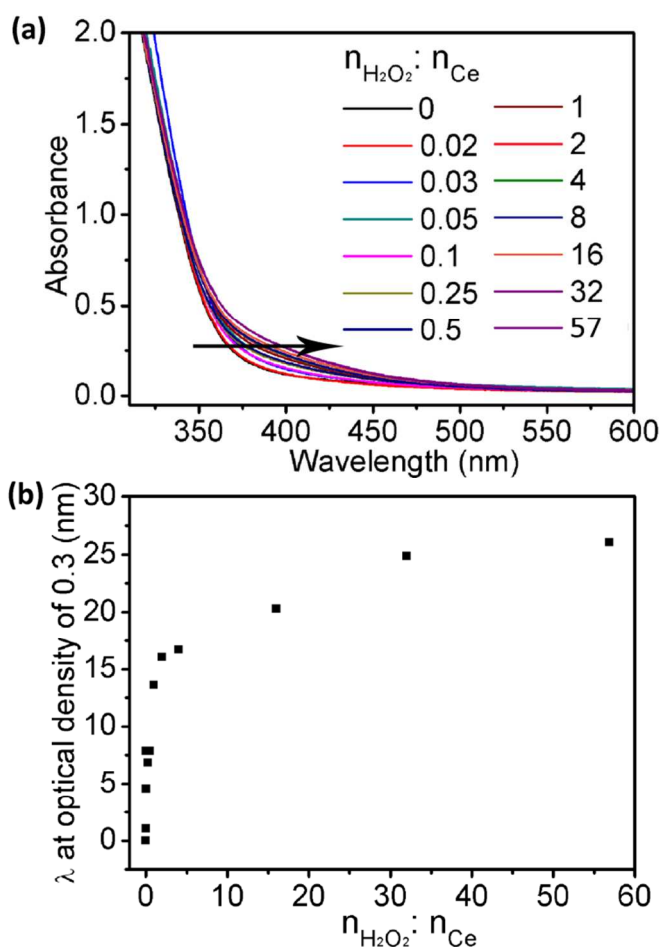


Fig. 2 Anti-oxidation reaction between CeO<sub>2</sub> NPs and H<sub>2</sub>O<sub>2</sub> (a) UV-vis spectra of CeO<sub>2</sub> NPs after the addition of H<sub>2</sub>O<sub>2</sub> at different molar ratio of H<sub>2</sub>O<sub>2</sub>:Ce. (b).  $\Delta\lambda$  at

optical density of 0.3 after injection of  $\text{H}_2\text{O}_2$  at different molar ratio of  $\text{H}_2\text{O}_2:\text{Ce}$ . ( $\Delta\lambda$ : the magnitude of the red-shifted wavelength of the UV-vis band was calculated between the control (molar ratio of  $\text{H}_2\text{O}_2:\text{Ce}$  was 0) and the red-shifted spectra at optical density of 0.3.

NPs.<sup>50,51</sup> According to previous reports, surface  $\text{Ce}^{3+}$  in  $\text{CeO}_2$  NPs can be stoichiometrically oxidized to  $\text{Ce}^{4+}$ , thus leading to the red-shifted absorption spectra of  $\text{CeO}_2$  NPs.<sup>26</sup> However, as we have confirmed in the EELS analysis above, the percentage of bulk  $\text{Ce}^{3+}$  in as-prepared  $\text{CeO}_2$  NPs is about 15%. In addition, XPS analysis exhibits no obvious observation of surface  $\text{Ce}^{3+}$  in as-prepared  $\text{CeO}_2$  NPs due to the synthesis in oxygen-enriched environment. Therefore, When the molar ratios of  $\text{H}_2\text{O}_2:\text{Ce}$  is 57.0, the molar ratios of  $\text{H}_2\text{O}_2:\text{Ce}^{3+}$  is estimated more than 350. Therefore, the red-shifted absorption in the presence of excessive  $\text{H}_2\text{O}_2$  is proposed to be not resulted from the oxidation of  $\text{Ce}^{3+}$ . As known, the absorption of  $\text{CeO}_2$  NPs in the UV region comes from O 2p to Ce 4f, which is closely related to the coordination environment of Ce. Therefore, the gradually increased red-shift of absorption spectra with  $\text{H}_2\text{O}_2$  concentration of as-prepared  $\text{CeO}_2$  NPs may mainly be attributed to the adsorption of peroxides species, thus lead to the color change of  $\text{CeO}_2$  solution.<sup>46</sup> We carried out further analyses for verification.

To quantitatively probe the local coordination structures of Ce ions in  $\text{CeO}_2$  NPs, X-ray absorption fine structure (XAFS) measurements were carried out. The time-dependent  $L_3$ -edge X-ray absorption near edge structures (XANES) spectra of Ce ions (Fig. S6) were recorded during the reaction between  $\text{CeO}_2$  NPs and  $\text{H}_2\text{O}_2$ . It can be found that the valence state of Ce ions in as-prepared  $\text{CeO}_2$  NPs is mainly +4 before and after the addition of  $\text{H}_2\text{O}_2$ , which agrees well with the XPS results. Table 1 shows the coordination number (CN), average coordinated Ce–O interatomic distance ( $R$ ), levels of disorder of oxygen ( $\sigma^2$ ) in  $\text{CeO}_2$  NPs. These results were fitted from the  $\kappa^2$ -weighted extended X-ray absorption fine structure (EXAFS) Fourier transform (FT) magnitude spectra, as shown in Fig. 3.

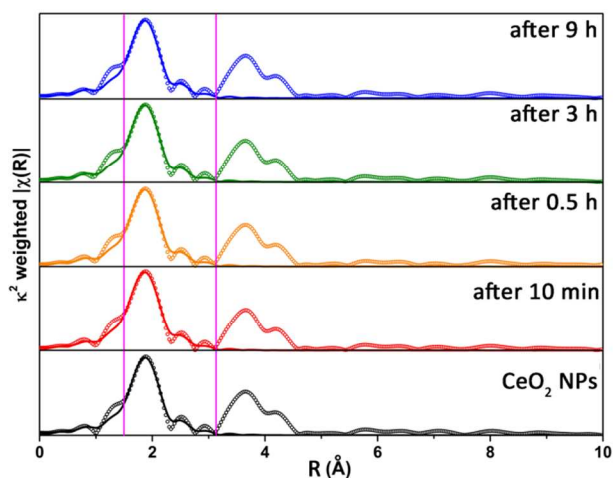


Fig. 3 EXAFS measurement during the reaction between  $\text{CeO}_2$  NPs and  $\text{H}_2\text{O}_2$ . Time-dependent  $\kappa^2$ -weighted EXAFS Fourier transform (FT) magnitude spectra recorded during the reaction.

Table 1 EXAFS results of  $\text{CeO}_2$  NPs during the anti-oxidation process

Sample.	Shell	CN	$R/\text{\AA}$	$\sigma^2/\text{\AA}^2$
$\text{CeO}_2$	Ce-O	$5.4\pm 0.2$	$2.320\pm 0.004$	$0.006\pm 0.001$
10 min	Ce-O	$6.2\pm 0.2$	$2.321\pm 0.005$	$0.008\pm 0.001$
0.5 h	Ce-O	$5.7\pm 0.2$	$2.319\pm 0.005$	$0.007\pm 0.001$
3 h	Ce-O	$5.5\pm 0.2$	$2.321\pm 0.005$	$0.006\pm 0.001$
9 h	Ce-O	$5.5\pm 0.2$	$2.320\pm 0.005$	$0.006\pm 0.001$

The CN value of  $\text{Ce}^{4+}$  is  $5.4\pm 0.2$  before the reaction, which is consistent with reduced CN of nanosized  $\text{CeO}_2$  due to the coordinatively unsaturated  $\text{Ce}^{4+}$  reported in previous research.<sup>18,23</sup> It increases to  $6.2\pm 0.3$  after  $\text{H}_2\text{O}_2$  addition. Considering the XAFS is a bulk technique, the slight increase in coordination number is proposed to be due to the averaged change mainly resulted from that of the surface Ce. The coordination number recovers back nearly to the initial value as the reaction proceeds (9 h). The increase of coordination number of  $\text{CeO}_2$  NPs was considered to be resulted from the emergence of the adsorbed oxygen species due to the coordination between Ce and  $\text{H}_2\text{O}_2$  during the anti-oxidation process.<sup>46</sup> We further carried out the study on the *in situ* Raman spectra of  $\text{CeO}_2$  NPs during the anti-oxidation process for verification.

The proposed adsorbed oxygen species in  $\text{CeO}_2$  NPs were probed by Raman spectroscopy under 488 nm laser excitations. Fig. 4 shows the *in situ* Raman spectra following the reaction between  $\text{CeO}_2$  NPs and  $\text{H}_2\text{O}_2$ . As known, the F2g peak can be indexed as a symmetric breathing mode of the oxygen atoms around Ce ions, which is sensitive to the disorder in the oxygen sublattice.<sup>47-49</sup> After the addition of  $\text{H}_2\text{O}_2$ , several new peaks centered at 860 and 880  $\text{cm}^{-1}$  immediately appear, which can be assigned to the O–O stretching of adsorbed peroxide species ( $\text{O}_2^{2-}$ ) with different degrees of defect aggregation.<sup>47-49</sup> This phenomenon is consistent with the increase of coordination number and levels of disorder of oxygen at 10 min obtained from the EXAFS measurement. After 30 min, the peak at 880  $\text{cm}^{-1}$  disappears, while the peak at 860  $\text{cm}^{-1}$  becomes weak progressively, and almost disappears after 3 h. Here, the peak intensity of adsorbed oxygen species from generation to disappearance is considered to be an anti-oxidation cycle. As anticipated, similar anti-oxidation processes are observed in the Raman spectra in the second and third cycles (Fig. S7 in ESI†). The cyclic catalytic property of anti-oxidative  $\text{CeO}_2$  NPs was visualized by Raman spectroscopy for the first time. Combined with the results obtained from EXAFS measurement, it can be deduced that the anti-oxidation process of  $\text{CeO}_2$  NPs is mainly accompanied by the increased CN after the addition of  $\text{H}_2\text{O}_2$  due to the emergence of coordinated peroxide species ( $\text{O}_2^{2-}$ ). Therefore, we propose that the coordination sites for peroxides species on the surface are the critical factor in the anti-oxidation process of  $\text{CeO}_2$  NPs with  $\text{H}_2\text{O}_2$ . In this regard, coordinated peroxides species probably have an effect on the color change of  $\text{CeO}_2$  NPs during the reaction with  $\text{H}_2\text{O}_2$ .

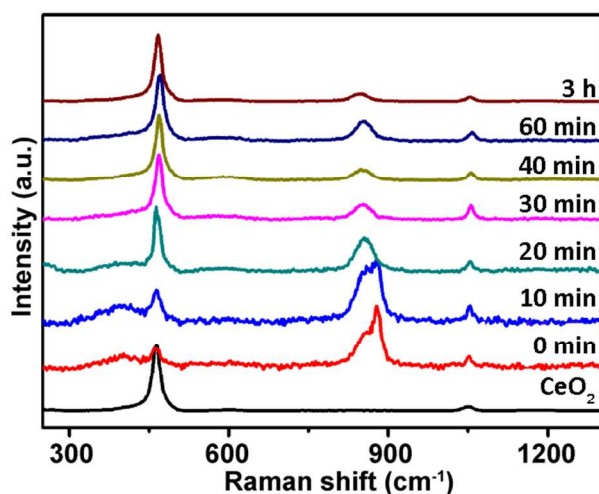
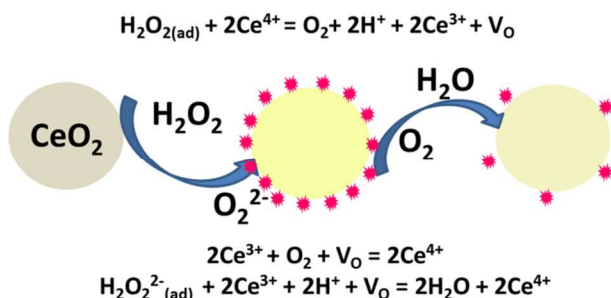


Fig. 4 Raman spectra of CeO<sub>2</sub> NPs during the reaction with H<sub>2</sub>O<sub>2</sub>.



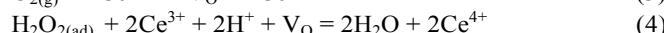
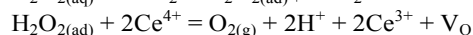
Scheme 1 Proposed anti-oxidation process of CeO<sub>2</sub> NPs with H<sub>2</sub>O<sub>2</sub>.

In addition, the hydroxyl radical ( $\cdot\text{OH}$ ), which is probably generated during the homolysis of H<sub>2</sub>O<sub>2</sub>, is harmful to human tissue. No significant  $\cdot\text{OH}$  can be observed during the anti-oxidation process of as-prepared CeO<sub>2</sub> NPs through ESR measurement (Fig. S8 in ESI†). Therefore, from the perspective of exploring biocompatible anti-oxidant, as-prepared CeO<sub>2</sub> NPs may be promising in further bio-application compared with other metal ions and oxides which can catalytically decompose H<sub>2</sub>O<sub>2</sub>.<sup>52-55</sup>

### Anti-oxidation mechanism of CeO<sub>2</sub> NPs

Based on the above results, we propose an anti-oxidation process of the as-prepared CeO<sub>2</sub> NPs (Scheme 1) as follows. First, peroxide species are coordinated onto the surface of CeO<sub>2</sub> NPs after H<sub>2</sub>O<sub>2</sub> addition, resulting in the red-shifted absorption spectra and the increase of coordination number of Ce (eq 1). Then, the interfacial redox reaction between CeO<sub>2</sub> and coordinated oxygen species is initiated, leading to the decrease of absorbed oxygen species, and the coordination number decreases accordingly. And oxygen vacancies (V<sub>O</sub>) may be generated with the formation of Ce<sup>3+</sup> (the reduction of Ce<sup>4+</sup>, eq 2). They are released with the oxidation of Ce<sup>3+</sup> (eq 3 or eq 4). Therefore, the active centres for the anti-oxidation process are proposed mainly to be determined by the surface Ce sites that can coordinate with oxygen species. On this basis, coordination capability of reaction sites for peroxides species and redox

ability of coordinated Ce sites may play critical role in the anti-oxidation performance of CeO<sub>2</sub> NPs.



Moreover, the investigation on the change in pH value of CeO<sub>2</sub> NPs solution further verified the proposed anti-oxidation mechanism. Reduced pH value was observed after adding H<sub>2</sub>O<sub>2</sub> into CeO<sub>2</sub> NP solution (from 8.1 to 6.0), indicating the generation of H<sup>+</sup> at the beginning of the reaction. We further studied the effect of extra OH<sup>-</sup> or H<sup>+</sup> on the anti-oxidation performance of CeO<sub>2</sub> NPs. Known from Fig. 5, extra OH<sup>-</sup> can slightly enhance the catalytic ability of decomposing H<sub>2</sub>O<sub>2</sub>. However, extra H<sup>+</sup> inhibits the decomposition of H<sub>2</sub>O<sub>2</sub>. According to proposed anti-oxidation mechanism, this phenomenon is probably because that extra OH<sup>-</sup> can slightly accelerate the reduction of Ce<sup>4+</sup> (eq 2) and extra H<sup>+</sup> can retard the reduction of Ce<sup>4+</sup> (eq 2). Therefore, we propose that reduction of Ce<sup>4+</sup> (eq 2), that is, the reducibility of CeO<sub>2</sub> NPs, is rate-determining step in the catalytic cycle. Therefore, the catalytic decomposition of H<sub>2</sub>O<sub>2</sub> closely depends on the reducibility of CeO<sub>2</sub> NPs. On the other hand, the oxidation of Ce<sup>3+</sup> to Ce<sup>4+</sup> (eq 3 and eq 4) is facile under oxygen-enriched environment. In previous reports, Ce<sup>3+</sup> on the surface can stoichiometrically react with H<sub>2</sub>O<sub>2</sub>.<sup>10,32,36,56-59</sup> When H<sub>2</sub>O<sub>2</sub>:Ce<sup>3+</sup> is 2:1, The anti-oxidation process can be anticipated for Fenton-type process and 1:1 or 1:2 for direct redox reactions.<sup>31</sup> According to as-proposed anti-oxidation mechanism, Ce<sup>3+</sup> can react with H<sub>2</sub>O<sub>2</sub>, thus is oxidized to Ce<sup>4+</sup>, just as previous reports have indicated. However, with excess H<sub>2</sub>O<sub>2</sub>, the regeneration of Ce<sup>3+</sup> (that is, the reduction of Ce<sup>4+</sup>) would be the key step in the catalytic cycle. Based on these experimentation and discussion above, the anti-oxidation performance of as-prepared CeO<sub>2</sub> NPs is due to the redox ability of coordinated Ce sites for peroxides species. For the current system, the ability of catalytically decomposing H<sub>2</sub>O<sub>2</sub> is attributed to the reducibility of CeO<sub>2</sub>.

### Anti-oxidation performance of CeO<sub>2</sub> and CeO<sub>2</sub>:Gd NPs

Based on the understanding of anti-oxidation mechanism, rational design and modulation of active sites to enhance the anti-oxidation activity of catalysts are significant in the anti-oxidation application of CeO<sub>2</sub> NPs. Engineering the surface defects of the catalysts is an efficient method to achieve enhanced performance.<sup>60-62</sup> As doping is an efficient method to delicately alter chemical activities of CeO<sub>2</sub> NPs,<sup>18,63,63</sup> we tuned anti-oxidation by doping Gd<sup>3+</sup> into CeO<sub>2</sub> NPs in this work. CeO<sub>2</sub>:Gd NPs were prepared by the same method with pure CeO<sub>2</sub> NPs.<sup>39</sup> Known from the XRD patterns (Fig S9), TEM images (Fig S10), size distribution (Fig S1) and hydrodynamic diameter (Fig S11) of as-prepared samples in ESI†, there is no obvious difference in phase, morphology and size between CeO<sub>2</sub>:Gd and CeO<sub>2</sub> NPs. In addition, the detailed characterizations about lattice parameter and interplanar spacing (*d*) of as-prepared CeO<sub>2</sub>-based NPs were shown in Table

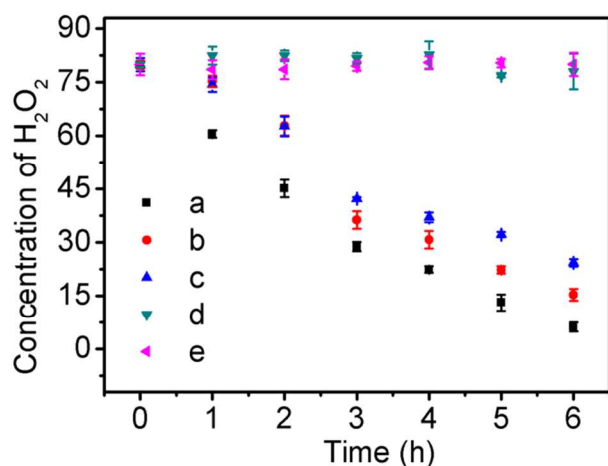


Fig. 5 The effect of extra  $\text{OH}^-$  or  $\text{H}^+$  on anti-oxidation capacity of  $\text{CeO}_2$  NPs. a  $\text{CeO}_2$  NPs + 2.5mM  $\text{OH}^-$ , b  $\text{CeO}_2$  NPs + 0.25mM  $\text{OH}^-$ , c  $\text{CeO}_2$  NPs, d  $\text{CeO}_2$  NPs + 0.25 mM  $\text{H}^+$ , e  $\text{CeO}_2$  NPs + 2.5 mM  $\text{H}^+$ . (extra  $\text{OH}^-$  is from NaOH, and extra  $\text{H}_2\text{SO}_4$ )

S1 in ESI†. XPS data further identify the percentage of  $\text{Gd}^{3+}$  in the surface layers and the valence state of Ce in  $\text{Gd}^{3+}$  doped NPs. For  $\text{CeO}_2:\text{Gd}$  NPs, the  $\text{Gd}^{3+}/\text{Ce}^{4+}$  ratio in the surface layers determined by XPS agrees well with the ICP-AES results (Table S1 in ESI†), indicating that the elemental distribution of  $\text{Gd}^{3+}$  is homogeneous. From Ce 3d XPS spectra shown in Fig. S3, three as-prepared  $\text{CeO}_2$ -based NPs show similar spectral profiles. No obvious difference about  $\text{Ce}^{3+}$  between  $\text{CeO}_2$  and  $\text{CeO}_2:\text{Gd}$  NPs was observed fitting Ce 3d XPS spectra in Fig S4 in ESI†. Furthermore, Fig. 6 shows the Raman spectra of the  $\text{CeO}_2$  and  $\text{CeO}_2:\text{Gd}$  NPs measured under 488 nm laser excitation. The Raman spectra of  $\text{CeO}_2$  NPs were dominated by the strong Raman-active vibrational mode (F2g) of the  $\text{CeO}_2$  fluorite phase at  $465\text{ cm}^{-1}$ , while the weak band at  $1050\text{ cm}^{-1}$  also existed due to the residual  $\text{NO}_3^-$ . Compared to  $\text{CeO}_2$  NPs, the peaks at  $550\text{ cm}^{-1}$  and  $600\text{ cm}^{-1}$  for  $\text{CeO}_2:\text{Gd}$  NPs are enhanced, due to the defect-induced (D1) mode, and the  $\text{GdO}_8$ -type complex (D2) mode, respectively. The amount of oxygen vacancies ( $I_{\text{D1}}/I_{\text{F2g}}$ ) (Table S1 in ESI†) increases with the ratio of  $\text{Gd}^{3+}$  doping.<sup>65</sup> Based on the characterization results above, it can be concluded that  $\text{Gd}^{3+}$  doping is successful.

The ability of decomposing  $\text{H}_2\text{O}_2$  of as-prepared  $\text{CeO}_2$  and  $\text{CeO}_2:\text{Gd}$  NPs was shown in Fig. 7. All  $\text{CeO}_2$ -based NPs exhibit excellent catalytic activities in  $\text{H}_2\text{O}_2$  scavenging compared with control ( $\text{H}_2\text{O}$ ). The turnover frequency (TOF) data of  $\text{CeO}_2$  and  $\text{CeO}_2:\text{Gd}$  NPs are shown in Table S2 in ESI†.  $\text{CeO}_2:\text{Gd}$  NPs show improved ability of decomposing  $\text{H}_2\text{O}_2$ . Further evidence about the modification by  $\text{Gd}^{3+}$  doping is revealed in the shift of absorption spectra. Referring to the previous reports,<sup>32,36</sup> the extent of red shift in absorption spectra is closely linked to the anti-oxidation performance. The absorption spectra of as-prepared  $\text{CeO}_2$  and  $\text{CeO}_2:\text{Gd}$  NPs before and after adding  $\text{H}_2\text{O}_2$  are shown in Fig. S11 in ESI†.  $\Delta\lambda$  at optical density of 0.3 was summarized in Table S3 in ESI† as the  $\text{H}_2\text{O}_2/\text{Ce}$  ratio is 57. It is evident that the extent of red shift in absorption spectra increases with the  $\text{Gd}^{3+}$  percentage in  $\text{CeO}_2$  NPs. Moreover, the coordination number of  $\text{CeO}_2:20\text{Gd}$  NPs following the reaction

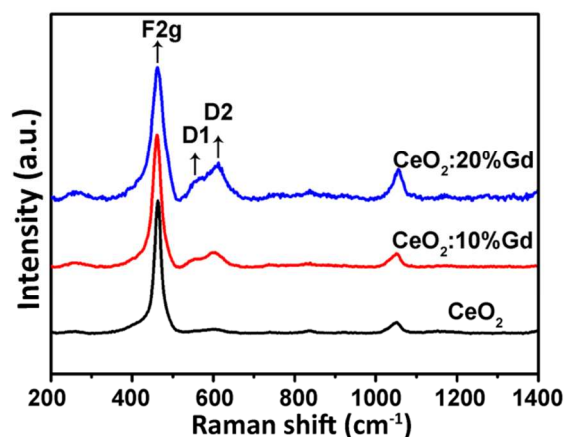


Fig. 6 Raman spectra of  $\text{CeO}_2$  NPs during the reaction with  $\text{H}_2\text{O}_2$ .

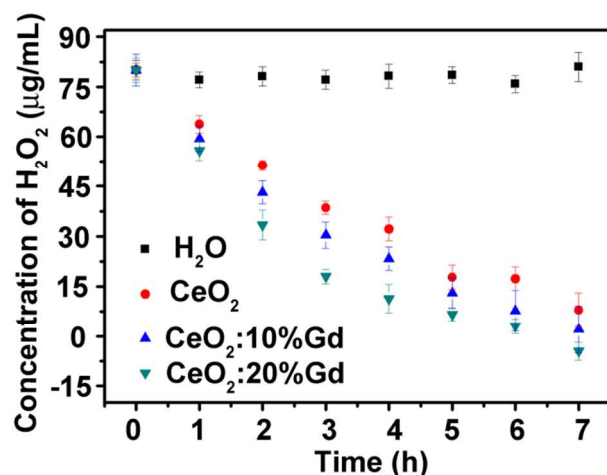


Fig. 7 The anti-oxidation ability of  $\text{CeO}_2$  and  $\text{CeO}_2:\text{Gd}$  NPs in the decomposition of  $\text{H}_2\text{O}_2$ . This experiment was repeated in triplicate.

was measured using XAFS spectroscopy, and the corresponding results were shown in Table S5. Compared with pure  $\text{CeO}_2$  NPs, an increased coordination number ( $6.4\pm 0.2$ ) is observed at the beginning of the reaction. This phenomenon is proposed to be due to the increased oxygen vacancies in  $\text{CeO}_2$  NPs after  $\text{Gd}^{3+}$  doping. Based on the discussion about the red shift and adsorbed peroxides species above, it can be concluded that coordination capability for adsorbed peroxides species increases following  $\text{Gd}^{3+}$  doping, which improves the reaction possibility of the  $\text{H}_2\text{O}_2$  decomposition due to the modification of defect state in as-prepared  $\text{CeO}_2$  based NPs.

As mentioned above, reduction of  $\text{Ce}^{4+}$  is a rate-determining step in the catalytic cycle of as-prepared  $\text{CeO}_2$  NPs. As confirmed from XPS data above, there is no obvious difference in surface  $\text{Ce}^{3+}$  percentage after doping  $\text{Gd}^{3+}$  in  $\text{CeO}_2$  NPs. Therefore, the change in surface bound-OH and reducibility of  $\text{CeO}_2$  NPs after doping  $\text{Gd}^{3+}$  was further investigated in order to understand this modification of anti-oxidation ability by  $\text{Gd}^{3+}$  dopant. From FT-IR analysis shown in Fig S8 in ESI†, it is unveiled that surface bound-OH on  $\text{CeO}_2$  NPs increases after  $\text{Gd}^{3+}$  doping. As known above,  $\text{OH}^-$  can improve the ability of decomposing  $\text{H}_2\text{O}_2$ . Therefore, increased surface bound-OH on

CeO<sub>2</sub> NPs after doping Gd<sup>3+</sup> may promote the decomposition of H<sub>2</sub>O<sub>2</sub>. In addition, H<sub>2</sub>-TPR measurement was carried out to understand the reducibility of as-prepared typical samples.<sup>18,66</sup> From the H<sub>2</sub>-TPR results shown in Fig. S12 in ESI†, the reducibility of CeO<sub>2</sub> NPs is observed to increase after doping Gd<sup>3+</sup>. Furthermore, the anti-oxidation performance of as-prepared CeO<sub>2</sub> NPs for the third catalytic cycle was measured and the TOF was shown in Table S4 in ESI†. CeO<sub>2</sub>:Gd NPs also showed improved anti-oxidation in cycling behavior. Therefore, the improved ability of decomposing H<sub>2</sub>O<sub>2</sub> after Gd<sup>3+</sup> doping may result from the accelerated reduction of Ce<sup>4+</sup> in catalytic cycle due to the increased surface bound-OH and enhanced reducibility of CeO<sub>2</sub> NPs.

On this basis, peroxide species are proposed can coordinate with surface Ce ions and decompose because of the intrinsic redox ability of Ce<sup>3+</sup>/Ce<sup>4+</sup> couples. When 20% of Gd<sup>3+</sup> was doped, the increased oxygen vacancies aroused by Gd doping increased the coordination capability of Ce sites for peroxide species and accelerated the reduction of Ce<sup>4+</sup> in the catalytic cycle of CeO<sub>2</sub> NPs. Consequently, the reaction possibility of the H<sub>2</sub>O<sub>2</sub> decomposition at the surface Ce sites around the dopants increased. Therefore, the improvement of anti-oxidation performance by Gd<sup>3+</sup> doping is proposed attributed to the delicate modulation in reaction sites for H<sub>2</sub>O<sub>2</sub>. This improvement of anti-oxidation performance of CeO<sub>2</sub>:Gd NPs was further observed in cell culture.

#### CeO<sub>2</sub> NPs protecting INS-1 cells from H<sub>2</sub>O<sub>2</sub> induced oxidative stress

The treatment of diabetes is challenging and meaningful for human health. As reported, diabetes is usually caused by dysfunction and apoptosis of INS-1 cells due to oxidative stress.<sup>3</sup> Oxidative stress plays a key role in the progress of diabetes because of weaker anti-oxidation capability of INS-1 cells. Anti-oxidant therapy has been paid great attention in treating diabetes for years.<sup>8</sup> Previous studies showed that ceria NPs, which act as potential anti-oxidants, were well tolerated by the organism, and exhibited anti-inflammatory properties and so on.<sup>25-27,67,68</sup> However, few studies have reported on the application of protecting INS-1 cells from oxidative stress with CeO<sub>2</sub> NPs. Here, the protection application of as-prepared CeO<sub>2</sub> NPs in INS-1 cells was investigated.

From the *in vitro* cytotoxicity of CeO<sub>2</sub> NPs on INS-1 cells shown in Fig. S14 in ESI†, no obvious decrease in cell viability is observed, confirming excellent biocompatibility of as-prepared CeO<sub>2</sub>-based NPs when the concentration ranges from 2 µg/mL to 500 µg/mL. Fig 8 shows the anti-oxidation protection of CeO<sub>2</sub> NPs and CeO<sub>2</sub>:Gd NPs on INS-1 cells incubated with H<sub>2</sub>O<sub>2</sub>. The cell viability of H<sub>2</sub>O<sub>2</sub> group is 60% compared with the control group. But the cell viability of 100 µg/mL CeO<sub>2</sub> NPs group approaches 100% under the same treatment, and the cell viability of CeO<sub>2</sub>:Gd group is higher than that of the pure CeO<sub>2</sub> group. Our research results show that CeO<sub>2</sub> NPs are excellent anti-oxidants to protect INS-1 cells from oxidative stress, indicative of the potential application in the treatment of diabetes.

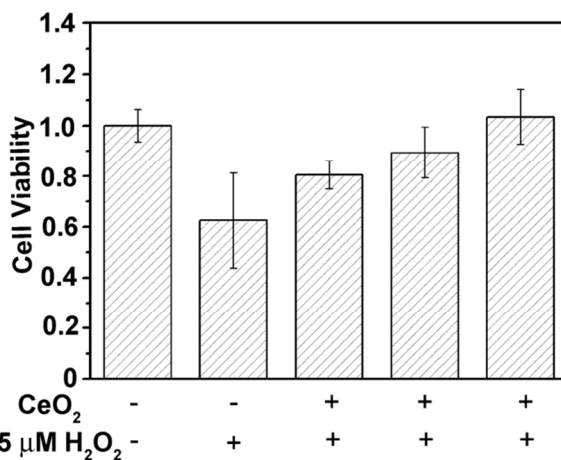


Fig. 8 CeO<sub>2</sub>-based NPs protecting INS-1 cells from H<sub>2</sub>O<sub>2</sub> induced oxidative stress. From left to right: control group, H<sub>2</sub>O<sub>2</sub> group, 100 µg/mL CeO<sub>2</sub> NPs + H<sub>2</sub>O<sub>2</sub> group, 100 µg/mL CeO<sub>2</sub>:10%Gd NPs + H<sub>2</sub>O<sub>2</sub> group, 100 µg/mL CeO<sub>2</sub>:20%Gd NPs + H<sub>2</sub>O<sub>2</sub> group.

#### Conclusions

In this work, we conducted detailed study on the anti-oxidation process of CeO<sub>2</sub> NPs and engineered the anti-oxidation performance of CeO<sub>2</sub> NPs by doping with Gd<sup>3+</sup>. Hydrophilic CeO<sub>2</sub>-based NPs without organic capping agents have been synthesized via a hydrothermal method. The red shift in UV-vis absorption spectra of CeO<sub>2</sub> NPs is observed after addition of H<sub>2</sub>O<sub>2</sub>, and the extent of red shift is found to be dependent on the concentration of H<sub>2</sub>O<sub>2</sub>. Moreover, time-dependent monitoring reveals that the coordination number of Ce ions increases after the addition of H<sub>2</sub>O<sub>2</sub>, and recovers back to nearly the initial value as the reaction proceeds. In addition, adsorbed oxygen species (O<sub>2</sub><sup>2-</sup>) generated during the anti-oxidation process are responsible for the red shift of absorption spectra. On the basis of these results, peroxide species are proposed to be able to coordinate with surface Ce ions and decompose because of the intrinsic redox ability of Ce<sup>3+</sup>/Ce<sup>4+</sup> pair. Moreover, the anti-oxidation performance of CeO<sub>2</sub> NPs is effectively improved by tuning the activity of coordinated Ce sites for peroxide species through the modulation of oxygen vacancies and reducibility after Gd<sup>3+</sup> doping. Our further experiments clearly show that the biocompatible CeO<sub>2</sub> and CeO<sub>2</sub>:Gd NPs are excellent anti-oxidants to protect INS-1 cells from being damaged by H<sub>2</sub>O<sub>2</sub> inducement, demonstrating that the CeO<sub>2</sub> NPs are promising candidates as potential anti-oxidants in the treatment of diabetes. In addition, our investigation may provide a universal way to optimize the anti-oxidation for further research by doping with other trivalent rare earth ions and obtain multifunctional CeO<sub>2</sub>-based nanomaterials (e. g. magnetic resonance imaging from Gd<sup>3+</sup>).

#### Acknowledgements

This work was supported by NSFC (Nos. 21331001, 21425101, 21371011, 21321001, 21461162001 and 91422302) and MOST of China (Nos. 2012CBA01204 and 2014CB643803). We thank the

beamline staff (1W2B of BSRF and BL14W1 of SSRF) and Mr. Lin-Dong Li for their aids on the ex-situ XAFS measurements. We highly appreciate the reviewers for their constructive suggestions that help us to improve our work.

### Notes and references

<sup>a</sup> Beijing National Laboratory for Molecular Sciences, State Key Laboratory of Rare Earth Materials Chemistry and Applications, PKU-HKU Joint Laboratory in Rare Earth Materials and Bioinorganic Chemistry, Peking University, Beijing 100871, China. Fax: +86-10-62754179; Tel: +86-10-62754179; Email: sun@pku.edu.cn, yan@pku.edu.cn.

<sup>b</sup> Key Laboratory for Advanced Battery Materials and System (MOE), School of Materials Science and Engineering, Huazhong University of Science and Technology (HUST), Wuhan, Hubei 430074, China. Fax: +86-27-87558241; Tel: +86-27-87558241; E-mail: huangyh@mail.hust.edu.cn.

<sup>c</sup> Department of Endocrinology, 306 Hospital of People's Liberation Army, Beijing 100101, China; Fax: +86-10-64860685; Tel: +86-10-66356374; E-mail: damaoermaosanmao@aliyun.com.

<sup>d</sup> Shanghai Synchrotron Radiation Facility, Shanghai Institute of Applied Physics, Chinese Academy of Sciences, Shanghai 201204, China.

<sup>e</sup> Beijing Synchrotron Radiation Facility, Institute of high energy physics, Chinese Academy of Sciences, Beijing 100049, China.

† Electronic Supplementary Information (ESI) available: Size distribution of prepared CeO<sub>2</sub>-based NPs, HRTEM of prepared CeO<sub>2</sub>-based NPs, XPS analysis of prepared CeO<sub>2</sub>-based NPs, EELS analysis of prepared CeO<sub>2</sub>-based NPs, TG curves and FT-IR spectra of CeO<sub>2</sub>-based NPs, XANES spectra of CeO<sub>2</sub> NPs during the reaction with H<sub>2</sub>O<sub>2</sub>, Raman spectrum of CeO<sub>2</sub> NPs during the reaction with H<sub>2</sub>O<sub>2</sub> for the second and third cycle, ESR analysis during the reaction, the red shift of UV-vis spectra of CeO<sub>2</sub>-based NPs after the addition of H<sub>2</sub>O<sub>2</sub>, H<sub>2</sub>-TPR test of CeO<sub>2</sub> and CeO<sub>2</sub>:20%Gd NPs, *In vitro* cytotoxicity of CeO<sub>2</sub>-based NPs in INS-1 cells.

- I. Celardo, J. Z. Pedersen, E. Traversa, and L. Ghibelli, *Nanoscale*, 2011, **3**, 1411-1420.
- T. Heitzer, T. Schlinzig, K. Krohn, T. Meinertz, and T. Münzel, *Circulation*, 2001, **104**, 2673-2678.
- A. C. Maritim, R. A. Sanders and J. B. Watkins, *J. Biochem. Mol. Toxic.*, 2003, **17**, 24-38.
- P. H. Chan, *J. Cerebr. Blood F. Met.*, 2001, **21**, 2-14.
- C. L. Allen and U. Bayraktutan, *Int. J. Stroke*, 2009, **4**, 461-470.
- G. C. Kujoth, A. Hiona, T. D. Pugh, S. Someya, K. Panzer, S. E. Wohlgenuth, T. Hofer, A. Y. Seo, R. Sullivan, W. A. Jobling, J. D. Morrow, H. Van Remmen, J. M. Sedivy, T. Yamsoba, M. Tanokura, R. Weindruch, C. Leeuwenburgh, and T. A. Prolla, *Science*. 2005, **309**, 481-484.
- B. G. Brown, X. Q. Zhao, A. Chait, L. D. Fisher, M. C. Cheung, J. S. Morse, A. A. Dowdy, E. K. Marino, E. L. Bolson, P. Alaupovic, J. Frohlich, and J. J. Albers, *New Engl. J. Med.*, 2001, **345**, 1583-1592.
- M. Valko, C. J. Rhodes, J. Moncol, M. Izakovic, and M. Mazur, *Chem-Biol. Interact.*, 2006, **160**, 1-40.
- M. Valko, D. Leibfritz, J. Moncol, M. T. Cronin, M. Mazur, and J. Telser. *Int. J. Biochem. Cell B*, 2007, **39**, 44-84.
- A. Karakoti, S. Singh, J. M. Dowding, S. Seal, and W. T. Self. *Chem. Soc. Rev.*, 2010, **39**, 4422-4432.
- N. J. Lawrence, J. R. Brewer, L. Wang, T. S. Wu, J. Wells-Kingsbury, M. M. Ihrig, G. Wang, Y. L. Soo, W. N. Mei, and C. L. Cheung, *Nano Lett.*, 2011, **11**, 2666-2671.
- C. Sun, and. D. Xue, *Phys. Chem. Chem. Phys.*, 2013, **15**, 14414-14419.
- J. Kašpar, P. Fornasiero, and M. Graziani, *Catal. Today*, 1999, **50**, 285-298.
- R. J. Gorte, *AIChE J.*, 2010, **56**, 1126-1135.
- C. Sun, H. Li, and L. Chen. *Energy Environ. Sci.*, 2012, **5**, 8475-8505.
- H. P. Zhou, Y. W. Zhang, R. Si, L. S. Zhang, W. G. Song, and C. H. Yan, *J. Phys. Chem. C*, 2008, **112**, 20366-20374.
- Z. L. Wang, and X. Feng, *J. Phys. Chem. B*, 2003, **107**, 13563-13566.
- J. Ke, J. W. Xiao, W. Zhu, H. Liu, R. Si, Y. W. Zhang, and C. H. Yan, *J. Am. Chem. Soc.*, 2013, **135**, 15191-15200.
- M. Nolan, and G. W. Watson, *J. Phys. Chem. B*, 2006, **110**, 16600-1666.
- Q. Yuan, H. H. Duan, L. L. Li, Z. X. Li, W. T. Duan, L. S. Zhang, W. G. Song, and C. H. Yan, *Adv. Mater.*, 2010, **22**, 1475-1478.
- Z. X. Li, L. L. Li, Q. Yuan, W. Feng, J. Xu, L. D. Sun, W. G. Song, and C. H. Yan, *J. Phys. Chem. C*, 2008, **112**, 18405-18411.
- D. Zhang, X. Du, L. Shi, and R. Gao, *Dalton Trans.*, 2012, **41**, 14455-14475
- Y. Sun, Q. Liu, S. Gao, H. Cheng, F. Lei, Z. Sun, Y. Jiang, H. Su, S. Wei, and Y. Xie, *Nat. Commun.*, 2013, **4**, 2899-907.
- S. M. Hirst, A. S. Karakoti, R. D. Tyler, N. Sriranganathan, S. Seal, and C. M. Reilly, *Small*, 2009, **5**, 2848-2856.
- S. Chen, Y. Hou, G. Cheng, C. Zhang, S. Wang, and J. Zhang, *Biol. Trace Elem. Res.*, 2013, **154**, 156-166.
- C. K. Kim, T. Kim, I. Y. Choi, M. Soh, D. Kim, Y. J. Kim, H. Jang, H. S. Yang, J. Y. Kim, H. K. Park, S. P. Park, S. Park, T. Yu, B. W. Yoon, S. H. Lee, and T. Hyeon, *Angew. Chem. Int. Ed.*, 2012, **51**, 1-6.
- J. Chen, S. Patil, S. Seal, and J. F. McGinnis, *Nat. Nanotechnol.*, 2006, **1**, 142-150.
- T. Pirmohamed, J. M. Dowding, S. Singh, B. Wasserman, E. Heckert, A. S. Karakoti, J. E. S. King, S. Seal, and W. T. Self, *Chem. Commun.*, 2010, **46**, 2736-2738.
- C. Korsvik, S. Patil, S. Seal, and W. T. Self, *Chem Commun.*, 2007, **10**, 1056-1058.
- E. G. Heckert, A. S. Karakoti, S. Seal, and W. T. Self, *Biomaterials*, 2008, **29**, 2705-2709.
- Y. Xue, Q. F. Luan, D. Yang, X. Yao, and K. Zhou, *J. Phys. Chem. C*, 2011, **115**, 4433-4438.
- S. S. Lee, W. Song, M. Cho, H. L. Puppala, P. Nguyen, H. Zhu, L. Segatori, and V. K. Colvin, *ACS Nano*, 2013, **7**, 9693-9703.
- I. Celardo, M. D. Nicola, C. Mandoli, J. Z. Pedersen, E. Traversa, and L. Ghibelli, *ACS Nano*, 2011, **5**, 4537-4549.
- X. Liu, W. Wei, Q. Yuan, X. Zhang, N. Li, Y. Du, G. Ma, C. Yan, and D. Ma, *Chem. Commun.*, 2012, **48**, 3155-3157.
- J. D. Cafun, K. O. Kvahnina, E. Casals, V. F. Puentes, and P. Glatzel, *ACS Nano*, 2013, **7**, 10726-10732.
- J. M. Perez, A. Asati, S. Nath, C. and Kaittanis, *Small*, 2008, **4**, 552-556.

- 37 A. S. Karakoti, S. Singh, A. Kumar, M. Malinska, S. V. N. T. Kuchibhatla, K. Wozniak, W. T. Self, and S. Seal, *J. Am. Chem. Soc.*, 2009, **131**, 14144-14145.
- 38 M. Spulber, P. Baumann, J. Liu, and C. G. Palivan, *Nanoscale*, 2015 (DOI: 10.1039/c4nr02748e).
- 39 H. X. Mai, L. D. Sun, Y. W. Zhang, R. Si, W. Feng, H. P. Zhang, H. C. Liu, and C. H. Yan, *J. Phys. Chem. B*, 2005, **109**, 24380-24385.
- 40 S. Turner, S. Lazar, S. Lazar, B. Freitag, R. Egoavil, J. Verbeeck, S. Put, Y. Struven, and G. V. Tendeloo, *Nanoscale*, 2011, **3**, 3385-3390.
- 41 B. Goris, S. Turner, S. Bals, and G. V. Tendeloo, *ACS nano*, 2014, **8**, 10878-10884.
- 42 Q. Yuan, H. H. Duan, L. L. Li, Z. X. Li, W. T. Duan, L. S. Zhang, W. G. Song, and C. H. Yan, *Adv. Mater.*, 2010, **22**, 1475-1478.
- 43 U. M. Bhatta, D. Reid, T. Sakthivel, T. X. T. Sayle, D. Sayle, M. Molinari, S. C. Parker, I. M. Ross, S. Seal, and G. Möbus, *J. Phys. Chem. C*, 2013, **117**, 24561-24569.
- 44 R. Wang, P. A. Crozier, and R. Sharma, *J. Phys. Chem. C*, 2009, **113**, 5700-5704.
- 45 D. G. Stroppa, C. J. Dalmaschio, L. Houben, J. Barthel, L. A. Montoro, E. R. Leite, and A. J. Ramirez, *Chem. Eur. J.*, 2014, **20**, 6288-6293.
- 46 F. H. Scholes, A. E. Hughes, S. G. Hardin, P. Lynch, and P. R. Miller, *Chem. Mater.*, 2007, **19**, 2321-2328.
- 47 Z. Wu, M. Li, J. Howe, H. M. Meyer, and S. H. Overbury, *Langmuir*, 2010, **26**, 16595-16606.
- 48 V. V. Pushkarev, V. I. Kovalchuk, and J. L. d'Itri, *J. Phys. Chem. B*, 2004, **108**, 5341-5348.
- 49 J. Guzman, S. Carettin, and A. Corma, *J. Am. Chem. Soc.*, 2005, **127**, 3286-3287.
- 50 Y. W. Zhang, R. Si, C. S. Liao, and C. H. Yan, *J. Phys. Chem. B*, 2003, **107**, 10159-10167.
- 51 K. Kuntaiah, P. Sudarsanam, B. M. Reddy, and A. Vinu, *RSC Adv.*, 2013, **3**, 7953-7962.
- 52 Z. Chen, J. J. Yin, Y. T. Zhou, Y. Zhang, L. Song, M. Song, S. Hu, and N. Gu, *ACS Nano*, 2012, **6**, 4001-4012.
- 53 J. Emerit, C. Beaumont, and F. Trivin, *Biomed. Pharmacother.*, 2001, **55**, 333-339.
- 54 L. J. Smith, A. L. Holmes, S. K. Kandpal, M. D. Mason, T. Z. Zheng, and J. P. Wise, *Toxicol. Appl. Pharm.*, 2014, **278**, 259-265.
- 55 L. Otero-González, C. García-Saucedo, J. A. Field, and R. Sierra-Álvarez, *Chemosphere*, 2013, **93**, 1201-1206.
- 56 E. Heckert, S. Seal, and W. T. Self, *Environ. Sci. Technol.*, 2008, **42**, 5014-5019.
- 57 C. Korsvik, S. Patil, S. Seal, and W. T. Self, *Chem. Commun.*, 2007, **10**, 1056-1058.
- 58 R. W. Tarnuzzer, J. Colon, S. Patil, and S. Seal, *Nano Lett.*, 2005, **5**, 2573-2577.
- 59 Y. Xue, Q. Luan, D. Yang, X. Yao, and K. Zhou, *J. Phys. Chem. C*, 2011, **115**, 4433-4438.
- 60 X. Liu, C. Meng, and Y. Han, *Nanoscale*, 2012, **4**, 2288-2295.
- 61 X. K. Gu, B. Qiao, C. Q. Huang, W. C. Ding, K. Sun, E. Zhan, T. Zhang, J. Liu, and W. X. Li, *ACS Catal.*, 2014, **4**, 3886-3890.
- 62 B. Qiao, A. Wang, X. Yang, L. F. Allard, Z. Jiang, Y. Cui, J. Liu, J. Li, and T. Zhang, *Nat. Chem.*, 2011, **3**, 634-641.
- 63 P. Fornasiero, G. Balducci, R. D. Monte, J. Kašpar, V. Sergo, G. Gubitosa, A. Ferrero, and M. Graziani, *J. Catal.*, 1996, **164**, 173-183.
- 64 R. Si, Y. W. Zhang, S. J. Li, B. X. Lin, and C. H. Yan, *J. Phys. Chem. B*, 2004, **108**, 12481-12488.
- 65 T. Taniguchi, T. Watanabe, N. Sugiyama, A. K. Subramani, H. Wagata, N. Matsushita, and M. Yoshimura, *J. Phys. Chem. C*, 2009, **113**, 19789-19793.
- 66 W. Y. Hernández, O. H. Laguna, M. A. Centeno, and J. A. Odriozola, *J. Solid State Chem.*, 2011, **184**, 3014-3020.
- 67 G. M. Lyu, Y. J. Wang, R. Liu, L. D. Sun, Y. H. Huang, and C. H. Yan, *Scientia Sinica Chim.*, 2013, **43**, 1309-1321.
- 68 Y. J. Wang, R. Liu, G. M. Lyu, L. D. Sun, Y. H. Huang, and C. H. Yan, *J. Chin. Soc. Rare Earths*, 2014, **32**, 257-269.